Nanoscale

RSC Publishing

PAPER

View Article Online
View Journal | View Issue

Cite this: *Nanoscale*, 2013, **5**, 5637

Synthesis, characterization and optical properties of low nuclearity liganded silver clusters: $Ag_{31}(SG)_{19}$ and $Ag_{15}(SG)_{11}$†

Franck Bertorelle,[a] Ramzi Hamouda,[a] Driss Rayane,[a] Michel Broyer,[a] Rodolphe Antoine,*[a] Philippe Dugourd,[a] Lars Gell,[b] Alexander Kulesza,[c] Roland Mitrić‡[c] and Vlasta Bonačić-Koutecký*[bd]

Received 6th February 2013
Accepted 14th April 2013

DOI: 10.1039/c3nr00677h

www.rsc.org/nanoscale

We report a simple synthesis of silver:glutathione (Ag:SG) clusters using a cyclic reduction under oxidative conditions. Two syntheses are described which lead to solutions containing well-defined $Ag_{31}(SG)_{19}$ and $Ag_{15}(SG)_{11}$ clusters that have been characterized by mass spectrometry. The optical properties of silver:glutathione (Ag:SG) cluster solutions have been investigated experimentally. In particular, the solution containing $Ag_{15}(SG)_{11}$ clusters shows a bright and photostable emission. For $Ag_{31}(SG)_{19}$ and $Ag_{15}(SG)_{11}$ clusters, the comparison of experimental findings with DFT and TDDFT calculations allowed us to reveal the structural and electronic properties of such low nuclearity liganded silver clusters.

Introduction

Low nuclearity liganded metal nanoclusters (NCs) have gained significant attention because they bring new interesting properties due to the quantum confinement effect.[1,2] Hence, they exhibit unique optical,[3–5] electronic,[6,7] and structural properties.[8–11] The quest for the smallest liganded metal NCs in the last few years has led to a tremendous development with the aim to explore new routes for their synthesis. In particular it is now possible to produce small silver NCs with bright emission,[12] which is of considerable interest in sensing applications.[13,14]

Different routes have been proposed to synthesize silver clusters. The use of templates is one of the most extensively studied. DNA encapsulated silver clusters,[15–17] though highly polydispersed, present remarkable absorption and emission features throughout the visible region. Dendrimers[18] and proteins[19–22] are also promising templates for silver cluster formation. Ligands containing thiol groups are good candidates to stabilize metal NCs due to the strong interaction between sulfur and silver or gold atoms.[7,23] Largely applied to gold,[24] chemical routes for stabilization of nanoclusters using thiolated ligands were recently extended to silver. Kitaev and co-workers[25,26] pioneered this field using chiral thiols to prepare silver clusters by a single-stage procedure or by an etching procedure. More recently, Bigioni and co-workers[27] reported the synthesis of glutathione-stabilized magic-number silver cluster compounds and their characterization by mass spectrometry.[28] Mass spectrometry has played a pivotal role in the characterization of magic-numbered metal NCs.[29–31] In particular, high-quality ESI mass spectra of a prototype silver:glutathione (Ag:SG) cluster were obtained recently by Bigioni, and a first composition assignment for a ligand-protected Ag cluster of formula $(Ag_{32}(SG)_{19})$ has been proposed.[28] It was also found that (Ag:SG) clusters are fragile relative to the well-characterized $Au_{25}(SG)_{18}$ clusters.

The routes mentioned above often imply delicate purification processes. Therefore, there is a need for developing simple synthetic approaches to create well-defined clusters with narrow size distributions. Very recently, Lopez-Quintela and co-workers reported a single step synthesis of liganded Ag_5 and Ag_6 fluorescent clusters *via* an electrochemical method.[32,33] In this paper, we report synthesis of silver:glutathione (Ag:SG) clusters using a cyclic reduction under oxidative conditions. Two syntheses are described and lead to solutions containing well-defined $Ag_{31}(SG)_{19}$ and $Ag_{15}(SG)_{11}$ that have been characterized by mass spectrometry. The optical properties of silver:glutathione (Ag:SG) cluster solutions have been

[a]*Institut Lumière Matière, UMR5306 Université Lyon 1-CNRS, Université de Lyon, 69622 Villeurbanne cedex, France. E-mail: rodolphe.antoine@univ-lyon1.fr; Fax: +33 4 72 43 15 07; Tel: +33 4 72 43 10 85*

[b]*Humboldt-Universität zu Berlin, Brook-Taylor-Straße 2, 12489 Berlin, Germany. E-mail: vbk@chemie.hu-berlin.de*

[c]*Department of Physics, Free University Berlin, Arnimallee 14, 14195 Berlin, Germany*

[d]*Center for Advanced Sciences and Technology (ICAST), University of Split, Meštrovićevo Šetalište bb., 2100 Split, Croatia*

† Electronic supplementary information (ESI) available: Optimal settings for the MS instrument; schematic diagrams for syntheses A and B; ESI mass spectra of silver clusters from "*synthesis A*" in different solvent mixtures, at different pH values and with different synthesis protocols; excitation and emission spectra of clusters from "*synthesis B*" in water and of the separated band after PAGE separation; lifetime measurements of silver clusters from a solution of "*synthesis B*" in water; the structure and absorption spectrum of the two lowest-energy isomers of $Ag_{15}(SCH_3)_{11}$. See DOI: 10.1039/c3nr00677h

‡ Present address: Institut für physikalische und theoretische Chemie, Julius-Maximilians Universität Würzburg, Emil-Fischer-Straße 42, 97074 Würzburg, Germany

investigated experimentally. In particular, the solution containing $Ag_{15}(SG)_{11}$ clusters shows a bright and photostable emission. For $Ag_{31}(SG)_{19}$ and $Ag_{15}(SG)_{11}$ clusters, the comparison of experimental findings with DFT and TDDFT calculations allowed us to reveal the structural and electronic properties of such low nuclearity liganded silver clusters.

Materials and methods

Materials

All the chemicals were commercially available and were used without purification. Triethylamine, methanol (HPLC grade), acrylamide (98%), bis-acrylamide (98%), glycine, tris(hydroxymethylamine) and GSH (γ-Glu-Cys-Gly, MW 307) were purchased from Carl Roth. $AgNO_3$, CF_3COOAg, glacial acetic acid, sodium borohydride ($NaBH_4$) and tetramethylammonium borohydride ($(CH_3)_4BH_4$) were purchased from Sigma Aldrich. MilliQ water with a resistivity of 18.2 MΩ cm was used for all experiments.

Synthesis and separation of low nuclearity liganded silver clusters

Synthesis A. This synthesis uses a cyclic reduction under oxidative conditions[26] and the following steps (the schematic diagram summarizing the synthesis steps is given in Scheme S1 in the ESI†).

(1) To an ice-cold solution of glutathione (200 mg GSH in 35 ml of H_2O) was added drop by drop 1 ml of $AgNO_3$ solution (55 mg ml^{-1}). A white precipitate appeared that was dispersed by adding 800 μl of 1 M NaOH solution (final pH ≈ 6–7). Then 36 mg of $NaBH_4$ in 1 ml of ice-cold water was quickly added and the solution was left under strong agitation.

(2) After 1 h 30 min, 300 μl of hydrogen peroxide (33%) was added to the dark brown solution.

(3) 30 min later, additional amounts of silver nitrate (140 μl at 100 mg ml^{-1}) and glutathione (50 mg per powder) were added and after 5 min, 500 μl of an ice-cold solution of $NaBH_4$ (20 mg ml^{-1}) was added. The reaction mixture was kept stirring vigorously for 1 h 30 min.

Steps (4–5) correspond to the purification process.

(4) Clusters were concentrated to a volume of ≈5 ml in a rotary evaporator ($T°$ ≈ 30 °C) before being precipitated by adding ≈15 ml of methanol and centrifuged for 5 min at 11 000 rpm. The supernatant was removed.

(5) Clusters were solubilised in 20 ml of water and 50 μl of glacial acetic acid was added (pH ≈ 4). The solution was left undisturbed 2 hours before being centrifuged for 30 min at 13 000 rpm. The precipitate was removed and the supernatant was concentrated as before. Clusters were precipitated with methanol and dried under vacuum. About 60–70 mg of brown powder was recovered.

Synthesis B. (1) 90 mg of glutathione was dissolved in methanol (40 ml) and triethylamine (1 ml). The solution was cooled in an ice bath and 0.5 ml of silver trifluoroacetate solution was added (64 mg ml^{-1} in methanol) under agitation.

(2) The solution was irradiated with a commercial UV lamp ("black light" lamp type, λ_{max} 365 nm, 25 W) and 50 mg (powder) of tetramethylammonium borohydride was quickly added.

Note that the only use of UV irradiation in the synthesis leads to a solution with the same optical properties as the one reported by Zhou *et al.*[34]

(3) After one hour the solution exhibited a strong red fluorescence. 20 mg (powder) of tetramethylammonium borohydride was added and the solution was agitated for one more hour.

Steps 4–5 correspond to the purification process.

(4) Clusters were concentrated to ≈5 ml in a rotary evaporator, precipitated by 15 ml of diethyl ether and centrifuged for 5 min (11 000 rpm).

(5) After being redissolved in water (≈1 ml) and 300 μl of NaOH (1 M) solution, 10 ml of methanol was added. The precipitate was centrifuged again (10 min/11 000 rpm). This cycle (dissolution/precipitation/centrifugation) was done 2 more times without NaOH. At the end, the powder was dried under vacuum. About 25–30 mg of a reddish powder was recovered.

Polyacrylamide gel electrophoresis (PAGE). PAGE separation was carried out using a vertical gel electrophoresis unit with a size of 0.2 cm × 20 cm × 20 cm. The separating and stacking gels were prepared by acrylamide monomers with the total contents of 35 and 7 wt% (acrylamide–bis-(acrylamide) 94 : 6), respectively. The eluting buffer consisted of 192 mM glycine and 25 mM tris(hydroxymethylamine). The as-prepared Ag(SG) clusters were dissolved in a 15% (v/v) glycerol–water solution (6 mg in 100 μl). The sample solutions were loaded onto the stacking gel (10 μl per well) and eluted for 7 h at a constant voltage mode (200 V) to achieve sufficient separation.

Mass spectrometry

Solutions were diluted without gel separation at a concentration of ~1 mg mL^{-1} in H_2O, electrosprayed at a flow rate of 10 μL min^{-1} and analyzed in negative mode with a linear quadrupole ion trap mass spectrometer (LTQ, Thermo Fisher Scientific, San Jose, CA) with a spray voltage of −3 kV and a capillary temperature of 100 °C. Other instrument settings were adjusted for each species to optimize the distribution of charge states observed in the mass spectrum. The optimal instrumental parameters for both cluster syntheses are given in Table S1 in the ESI.† Isotope-resolved mass spectra were recorded using the zoom scan mode of the instrument (mass resolution ~10 000, mass accuracy 0.2 Th).

Fluorescence measurements

Steady-state and lifetime measurements. Fluorescence excitation and emission spectra were measured using a fluoromax-4 Horiba fluorescence spectrophotometer, in the resolved time mode. Luminescence decay curves were collected with the time-correlated single-photon counting (TCSPC) extension of fluoromax-4 using a nano-led source (370 nm).

Quantum yield measurement. DCM in methanol (quantum yield 0.43)[35] was chosen as a standard. First of all, a series of different concentrations of DCM and silver nanoclusters were prepared. From the absorption spectrum, DCM and silver

nanoclusters were found to have a shared region of linear absorption as a function of concentration from 380 nm to 540 nm. 440 nm was chosen as the excitation wavelength. The emission intensities of DCM and silver nanoclusters were integrated from 500 nm to 800 nm. Both the excitation and emission slit apertures were 5 mm. Linear relationships between the absorption and the integrated emission intensity were observed with slopes of 7.86×10^8 and 8.19×10^7, for DCM and silver nanoclusters respectively. The quantum yield of silver nanoclusters is obtained using:

$$\varphi = \varphi_r \frac{A_r}{I_r} \frac{I}{A} \quad (1)$$

where φ is the quantum yield, I is the measured integrated emission intensity, A is the absorbance and the subscript "r" refers to the reference DCM.

Computational

The structural and optical properties of liganded clusters have been determined using density functional theory (DFT) and its time-dependent version (TDDFT).

For the silver atoms the 19-e$^-$ relativistic effective core potential (19-e$^-$ RECP) from the Stuttgart group[36] taking into account scalar relativistic effects has been employed. For all atoms triple zeta plus polarization atomic basis sets (TZVP) have been used.[36,37] Becke's three-parameter non-local exchange functional together with the Lee–Yang–Parr gradient-corrected correlation functional (B3LYP)[38–41] and its Coulomb-attenuated version (CAM-B3LYP)[42] have been employed to determine structural and optical properties of gas-phase liganded clusters.

An extensive search for structures of the silver complexes has been performed using the simulated annealing method coupled to molecular dynamics simulations in the frame of the semi-empirical AM1 method.[43] The found structures were then reoptimized in the frame of the DFT method using the functionals and AO basis sets as described above. The vibrational frequencies have been computed in order to find true minima on the potential energy surfaces.

Results and discussion

The nanoclusters produced by "*synthesis A*" and "*synthesis B*" were characterized by mass spectrometry and optical methods. As described in more detail below, "*synthesis A*" mainly leads to the magic-size nanocluster $Ag_{31}SG_{19}$, while "*synthesis B*" leads to smaller nanoclusters and in particular contains the size $Ag_{15}SG_{11}$. While nanoclusters produced by "*synthesis A*" are non-fluorescent, a strong fluorescence in the red is observed for nanoclusters produced by "*synthesis B*".

$Ag_{31}(SG)_{19}$

Fig. 1 shows the UV-vis absorption spectra in solution of the silver clusters synthesized using "*synthesis A*". An intense visible band centred at ~490 nm is observed. The present spectrum is very similar to the one reported by Bigioni *et al.* on the so-called "band 6".[27] "*Synthesis A*" leads to a unique band closely located near the "band 6" observed in Bigioni synthesis (see inset in Fig. 1). The absorption spectrum after gel separation is also displayed in Fig. 1. Absorption spectra in solution and the separated band after PAGE separation are very similar.

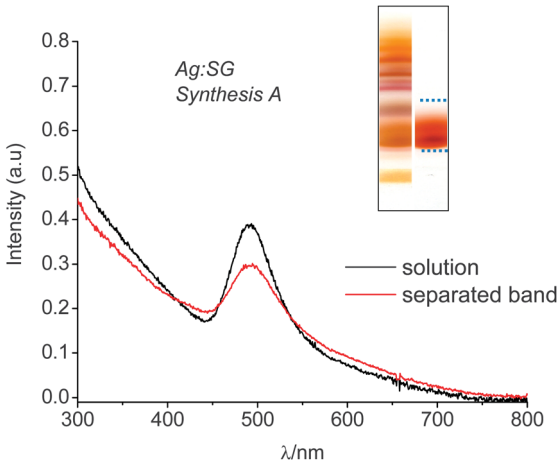

Fig. 1 UV-visible absorption spectra of silver nanoclusters. (Black line) Absorption spectrum of silver clusters from "*synthesis A*" in water solution. (Red line) Absorption spectrum of the band extracted after PAGE separation. Inset: PAGE for Ag:SG clusters using (left) Bigioni synthesis (see ref. 27) and (right) our "*synthesis A*". The part extracted for optical spectra (red line in the figure) was the one between the two dotted lines.

The size of the prepared silver clusters was estimated using ESI-mass spectrometry, which is a particularly useful technique in the case of silver due to its unequivocally isotopic patterns. An ESI mass spectrum of the silver–glutathione cluster from a solution of "*synthesis A*" and acquired under gentle ESI conditions is shown in Fig. 2. A charge state distribution was observed from $[M - 3H^+]^{3-}$ through $[M - 7H^+]^{7-}$. Deconvolution of charge states 3^- through 7^- provided a mass of 9161 Da

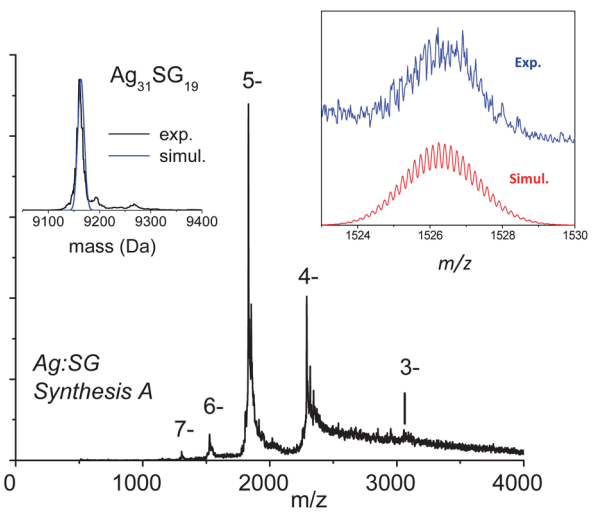

Fig. 2 ESI mass spectrum of silver clusters from "*synthesis A*". Right inset: comparison of the experimental and simulated isotopic distributions for the 6^- charge state of $Ag_{31}(SG)_{19}$. Left inset: comparison of the experimental and simulated deconvoluted spectra of $Ag_{31}(SG)_{19}$.

for the intact Ag cluster, consistent with the calculated mass of $Ag_{31}(SG)_{19}$ (see the left inset in Fig. 2). To verify this formula assignment, ESI spectra in zoom scan mode were recorded to obtain isotopic resolution. The measured mass distribution was compared with the simulated isotopic distributions for the 6^- charge state of $Ag_{31}(SG)_{19}$. Although not completely resolved, the isotopic distributions were found to be in good agreement (see the right inset in Fig. 2), thus confirming the molecular formula assignment. In fact, silver NCs are fragile which prevented the possibility of increasing the mass resolution of our instrument to the ultra-zoom scan mode. This size was already observed and reported by Bigioni and co-workers. However, in their synthesis, using gentle ESI conditions and solution conditions designed to stabilize the clusters, they observed mainly the $Ag_{32}(SG)_{19}$ ligand-protected Ag cluster. To better understand the origin of the discrepancy, we conducted additional MS measurements. In particular, we did MS experiments with different agitation speeds in synthesis steps (1–3), by varying the pH of the solution and by adding methanol. (i) Addition of methanol leads to an increase in the background noise and the appearance of additional peaks (see Fig. S1 in the ESI†). (ii) The pH affects the charge state distributions observed in mass spectra. Distributions are shifted to lower charge states for low pH. For pH > 9, an increase in the background noise is observed along with the appearance of additional peaks (see Fig. S2 in the ESI†). (iii) Interestingly, for pH = 3–4, in addition to the peak corresponding to the 4^- charge state of $Ag_{31}(SG)_{19}$, a small peak on the right is assigned to the cluster size $Ag_{32}(SG)_{19}$. The presence of the peak is strongly enhanced if MS experiments are conducted on clusters from *synthesis A* with moderate agitation speed in steps (1–3) (see Fig. S3 in the ESI†). Thus the ratio between $Ag_{31}(SG)_{19}$ and $Ag_{32}(SG)_{19}$ depends on the agitation speed during the synthesis (the role of oxygen may be important for the final ratio) and also the pH conditions.

$Ag_{15}(SG)_{11}$

Fig. 3 shows the UV-vis absorption spectra of the silver clusters synthesized using "*synthesis B*". The absorption spectrum displays a continuous increase below 600 nm with a plateau between 400 and 500 nm. The present absorption spectrum is very similar to the one reported by Bigioni *et al.* on the so-called "band 2".[27] The nanoclusters produced by "*synthesis B*" are fluorescent. An intense and broad luminescent emission band located at 690 nm is observed upon excitation at 470 nm (Fig. 3). This emission (excitation) band does not significantly vary with the excitation (emission) wavelength (see Fig. S4 in the ESI†). The luminescence quantum yield is measured to be 2.2 ± 1% relative to DCM dye (see the Experimental section for details). Once again, our synthesis "*synthesis B*" leads to a major band closely located near the "band 2" in Bigioni synthesis. The absorption spectrum after gel separation is displayed in Fig. S4 in the ESI.† Absorption, emission and excitation spectra in solution and after gel separation are very similar (see Fig. S4†). In order to have a better understanding of the excited-state dynamics, we performed picosecond time-resolved fluorescence decay measurements for silver clusters from "*synthesis B*". Results are given in Fig. S6 in the ESI.† The curve can be fitted by a double exponential curve (characteristic times of 0.75 ns and 3.6 ns). According to previous studies, the shorter decay corresponds to the emission of a charge transfer state, and longer decay (3.6 ns) comes from the emission of the Ag core.[32]

An ESI mass spectrum of the silver–glutathione cluster from a solution of "*synthesis B*" and acquired under gentle ESI conditions is shown in Fig. 4. Two charge states for silver NCs were observed ($[M - 4H^+]^{4-}$ and $[M - 3H^+]^{3-}$). Deconvolution of charge states provided a mass of 4987 Da for the intact Ag cluster, consistent with the calculated mass of $Ag_{15}(SG)_{11}$. The

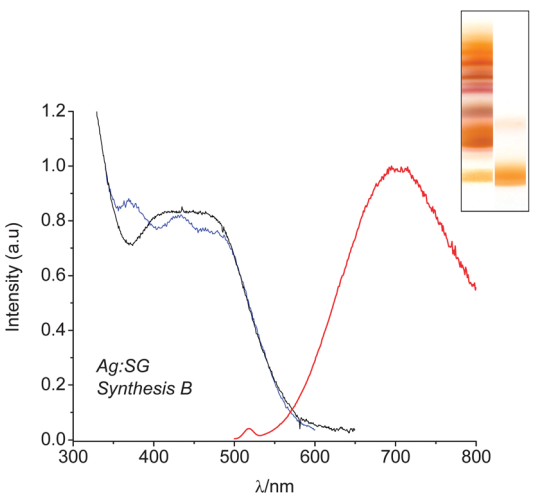

Fig. 3 Absorption, excitation and emission spectra of silver nanoclusters from "*synthesis B*" in water solution. (Black line) Absorption spectrum, (red line) emission spectrum with excitation at 470 nm, (blue line) excitation spectrum for emission at 665 nm. Inset: PAGE for Ag:SG clusters using (left) Bigioni synthesis (see ref. 27) and (right) our "*synthesis B*".

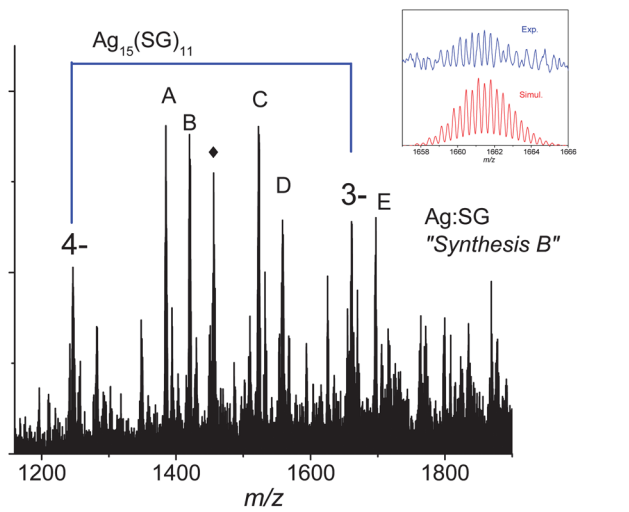

Fig. 4 ESI mass spectrum of silver clusters from "*synthesis B*". Inset: comparison of the experimental and simulated isotopic distributions for the 3^- charge state of $Ag_{15}(SG)_{11}$. Peaks labelled A, B, C, D and E correspond to clusters with the 3^- charge state of $Ag_{13}(SG)_9$, $Ag_{14}(SG)_9$, $Ag_{14}(SG)_{10}$, $Ag_{15}(SG)_{10}$ and $Ag_{16}(SG)_{11}$, respectively. The peak labelled by a black diamond corresponds to the cluster with 2^- charge state of $Ag_{10}(SG)_6$

peak attribution was confirmed by isotopic distribution measurement (see inset in Fig. 4).

Although $Ag_{15}(SG)_{11}$ was the most abundant NC observed in mass spectra of a solution of "*synthesis B*", other peaks are present and are due to $Ag_{14}(SG)_{10}$, $Ag_{14}(SG)_9$, $Ag_{13}(SG)_9$, $Ag_{15}(SG)_{10}$ and $Ag_{16}(SG)_{11}$. The presence of numerous small NCs in mass spectra of "*synthesis B*" may be due to a silver atom and/or ligand evaporation from $Ag_{16}(SG)_{11}$ and $Ag_{15}(SG)_{11}$ clusters in the ionic train of our MS instrument. Note that, after isolation and collision-induced activation with helium atoms in the trap, $Ag_{15}(SG)_{11}$ easily fragments by an evaporation of a charged or neutral glutathione molecule (leading to $Ag_{15}(SG)_{10}$) (data not shown).

Our results on the fluorescence properties (both emission band, quantum yield) of nanoclusters produced by "*synthesis B*" are close to the recent work of Le Guével *et al.*,[44] who also used glutathione to stabilize silver nanoclusters. However in ref. 44 such nanoclusters were produced using a delicate protocol by collecting them on a plastic surface during an interfacial etching process. Furthermore, the red emitting clusters were found to present larger polydispersity in cluster size with probable quenching due to the presence of non-fluorescent species. Finally, these red emitting clusters showed a long lifetime component (>100 ns). This long lifetime component may be related to the electronic transfer between the triplet excited state of the sp orbitals of silver and the p orbitals of sulfur.[45] Difference in lifetime decay observed between the present silver NCs and those reported by Le Guével *et al.*[44] is certainly due to differences in cluster size and/or staple ligand nature.

It is interesting to compare the size of the nanoclusters with their fluorescence properties. Indeed, quantum confinement can offer a qualitative explanation of fluorescence emission for noble metal clusters. However, many factors such as the oxidation state of the metal, the nature of the ligand, and the steric protection of the metal core affect the fluorescence properties. Small silver clusters (<10 atoms) have recently received significant attention due to their strong red fluorescence.[46–48] Red fluorescence is usually observed for NCs with less than 25 silver atoms,[19,26,49,50] although, red emission was recently reported for silver NCs assigned to $Ag_{75}(SG)_{40}$.[51] The silver NCs obtained with "*synthesis B*" present a high quantum yield as compared to other liganded clusters using organic templates; however the quantum yields for NCs using protein as a template are higher.[50]

Structural and optical properties of $Ag_{31}(SG)_{19}$ and $Ag_{15}(SG)_{11}$. Insight from theory

To rationalize the effect of thiolated liganded shells on structural and optical properties of silver clusters, we present theoretical results obtained for two prototype examples containing S–CH_3 ligands ($Ag_{15}(SCH_3)_{11}$ and $Ag_{31}(SCH_3)_{19}$). Since sulfur can be considered as an electron acceptor, each pair of Ag and S atoms formally consists of Ag^+ and S^-. Thus, by combining *n* silver atoms and *x* ligands the excess of Ag atoms determines the count of confined electrons, which is related to the "superatom" model used successfully for thiolate protected gold clusters.[11] The structure of the $Ag_{15}(SCH_3)_{11}$ cluster contains an Ag_8 core which is protected by four ligands belonging to three different types. Two ligands are of the type labelled L1 (CH_3S–Ag–SCH_3), one other ligand is of the type labelled L2 (CH_3S–Ag–SCH_3–Ag–SCH_3) and the fourth one is of the L3 type (CH_3S–Ag–SCH_3–Ag–SCH_3–Ag–SCH_3) as shown in Fig. 5 and 6. The structure of the $Ag_{31}(SCH_3)_{19}$ cluster contains an Ag_{21} core which is protected by nine ligands belonging to two different types: eight L1 ligands and one L2 ligand (as shown in Fig. 5 and 6). The number of electrons within the cluster core can be determined by examining the occupation of delocalized cluster orbitals which can be classified as S, P and D-like orbitals. For the $Ag_{15}(SCH_3)_{11}$ cluster, the fully ligand-protected Ag_8 core contains 4 confined electrons, while for $Ag_{31}(SCH_3)_{19}$, the core contains 12 confined electrons. Electron localization function (ELF) plots (displayed in Fig. 5c) show the localization of these electrons in the silver core. In $Ag_{15}(SCH_3)_{11}$ the four confined electrons occupy the lowest cluster S-orbital and a single cluster P-orbital while in $Ag_{31}(SCH_3)_{19}$ the S and P cluster orbitals are fully occupied and four additional electrons occupy two D-orbitals. These confined electrons play an important role in determining the spectroscopic pattern shown in Fig. 5a. The spectroscopic patterns of $Ag_{31}(SCH_3)_{19}$ are characterized by an intense transition at 510 nm due to excitations from the D-cluster-core orbital to the F-cluster-core-orbitals (Fig. 5b). The calculated spectrum is in good agreement with the experimental absorption spectrum (Fig. 1). The spectroscopic patterns of $Ag_{15}(SCH_3)_{11}$ are characterized by an intense transition at 410 nm due to excitations from the P-cluster-core orbital to the D-cluster-core-orbitals (Fig. 5b). A first band is calculated at 572 nm. Note that the position of this first band is very sensitive to the structures of isomers (as shown in Fig. S7 in the ESI†). Experimentally, we observe a plateau between 400 nm and 500 nm with an onset of absorption at ~600 nm (see Fig. 3 and S5†). We wish to emphasize that different cluster sizes (and possibly isomers) coexist in "*synthesis B*" (as evidenced by MS data), and the resulting absorption spectrum is a convolution of all spectroscopic patterns of individual clusters (between $Ag_{13}(SG)_9$ and $Ag_{16}(SG)_{11}$) which may smooth the lowest energy band and result in a regular increase as observed in Fig. 4. Emission spectra recorded for Ag_4 and Ag_3 clusters embedded in matrix[52] and aptamer templates[53] display visible fluorescence, while larger clusters only display fluorescence in the UV range. This is in agreement with the small number of confined electrons calculated for the $Au_{15}(SG)_{11}$ nanocluster.

Interestingly, the structure obtained for $Ag_{15}(SCH_3)_{11}$ differs significantly from the structure predicted for small thiolated gold clusters.[54] Indeed, the most stable geometries for $[Au_{12}(SCH_3)_9]^+$, $[Au_{13}(SCH_3)_{10}]^+$, $[Au_{14}(SCH_3)_{11}]^+$, and $[Au_{15}(SCH_3)_{12}]^+$ lead to structures with an Au_6 core covered with dimer $[Au_2(SCH)_3]$ and trimer $[Au_3(SCH_3)_4]$ motifs or their combinations. This family of gold NCs corresponds to a series of clusters that satisfy the $2e^-$ shell closing count, which is the smallest one within the spherical superatom complex model. Au(I) and Ag(I)-thiolate complexes lead to different stoichiometries (in particular silver tends to form larger complexes) due to differences in Au– and Ag–sulfur chemistry.[55] This may account for the formation of different metal cores and staple liganded complexes between small silver and gold nanoclusters.

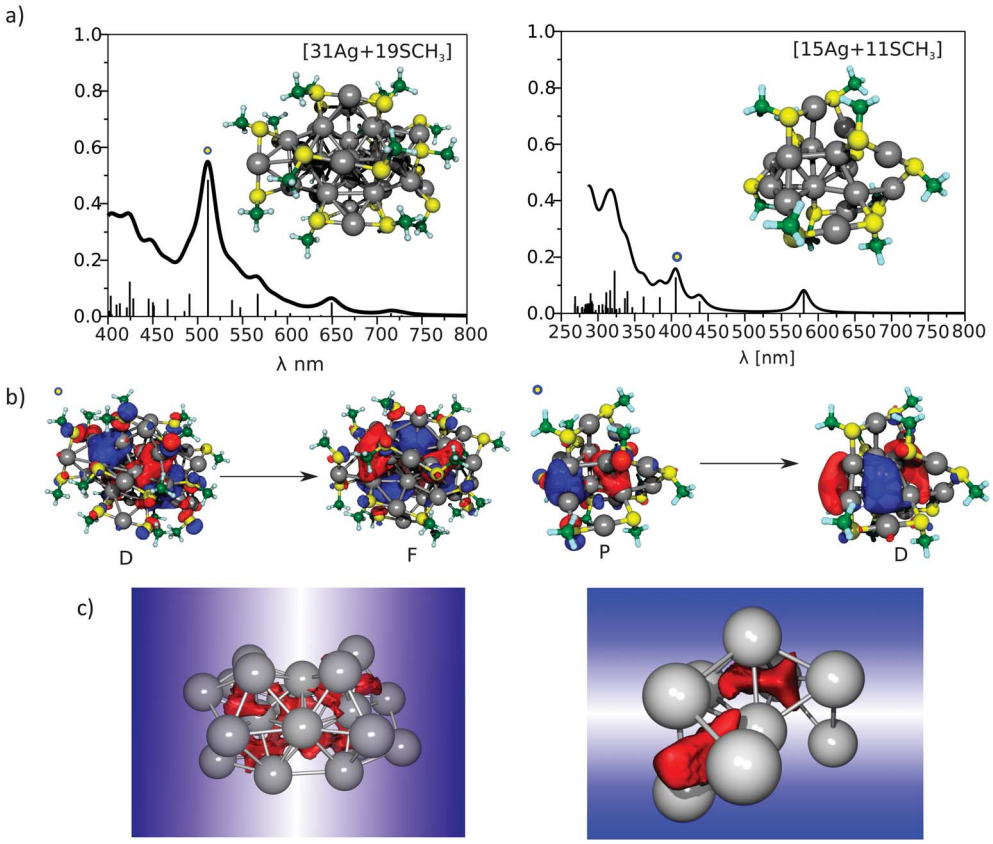

Fig. 5 (a) Structure and absorption spectrum of $Ag_{15}(SCH_3)_{11}$ and $Ag_{31}(SCH_3)_{19}$ clusters. (b) Analysis of transitions labelled by (o) in terms of leading excitations between Kohn–Sham orbitals. (c) Core structure of (left) $Ag_{31}(SCH_3)_{19}$ and (right) $Ag_{15}(SCH_3)_{11}$ clusters together with the electron localization function (ELF) plotted for the isovalue 0.20 for $Ag_{15}(SCH_3)_{11}$ and 0.25 for $Ag_{31}(SCH_3)_{19}$.

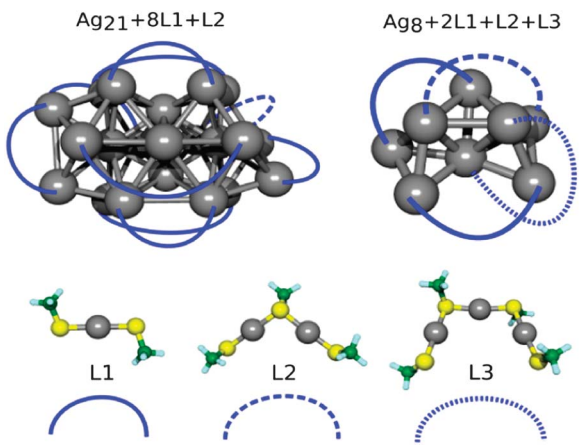

Fig. 6 Structure of the silver core for $Ag_{15}(SCH_3)_{11}$ and $Ag_{31}(SCH_3)_{19}$ for clusters with different types of ligands. L_n corresponds to the staple ligand types where n is the number of silver atoms.

Conclusions

We have reported a simple synthesis of silver:glutathione (Ag:SG) clusters using a cyclic reduction under oxidative conditions leading to a solution containing magic-numbered silver NCs. Insight from theory for structural and optical properties of ultrasmall silver NCs permits us to better address the nature of the metal core and the staple motifs that stabilize the silver core, and to outline the difference with small liganded gold nanoclusters. The solution containing $Ag_{15}(SG)_{11}$ clusters shows a bright and photostable emission. Such low nuclearity silver nanoclusters are potentially promising for biolabeling and imaging as alternatives to the standard fluorescent probes such as quantum dots or organic dyes.

Acknowledgements

Financial support from the Project "Laboratoire International Associé (LIA)" NCBA between France and Croatia is gratefully acknowledged. We acknowledge financial support of the Deutsche Forschungsgemeinschaft (DFG) in the frame of the Emmy Noether programme, MI-1236 (R.M.) and of the Research Unit FOR 1282 (V.B.-K. and R.M.). We are grateful to the ANR for financial support of this work (Grant No. ANR-08 BLAN-0110-01).

Notes and references

1 W. A. de Heer, *Rev. Mod. Phys.*, 1993, **65**, 611–676.
2 H. F. Qian, M. Z. Zhu, Z. K. Wu and R. C. Jin, *Acc. Chem. Res.*, 2012, **45**, 1470–1479.
3 K. L. Kelly, E. Coronado, L. L. Zhao and G. C. Schatz, *J. Phys. Chem. B*, 2003, **107**, 668–677.

4 M. M. Alvarez, J. T. Khoury, T. G. Schaaff, M. N. Shafigullin, I. Vezmar and R. L. Whetten, *J. Phys. Chem. B*, 1997, **101**, 3706–3712.
5 Y. Negishi, Y. Takasugi, S. Sato, H. Yao, K. Kimura and T. Tsukuda, *J. Am. Chem. Soc.*, 2004, **126**, 6518–6519.
6 C. M. Aikens, *J. Phys. Chem. Lett.*, 2010, **2**, 99–104.
7 R. C. Jin, *Nanoscale*, 2010, **2**, 343–362.
8 M. W. Heaven, A. Dass, P. S. White, K. M. Holt and R. W. Murray, *J. Am. Chem. Soc.*, 2008, **130**, 3754–3755.
9 S. W. Chen, R. S. Ingram, M. J. Hostetler, J. J. Pietron, R. W. Murray, T. G. Schaaff, J. T. Khoury, M. M. Alvarez and R. L. Whetten, *Science*, 1998, **280**, 2098–2101.
10 P. D. Jadzinsky, G. Calero, C. J. Ackerson, D. A. Bushnell and R. D. Kornberg, *Science*, 2007, **318**, 430–433.
11 M. Walter, J. Akola, O. Lopez-Acevedo, P. D. Jadzinsky, G. Calero, C. J. Ackerson, R. L. Whetten, H. Gronbeck and H. Hakkinen, *Proc. Natl. Acad. Sci. U. S. A.*, 2008, **105**, 9157–9162.
12 I. Diez and R. H. A. Ras, *Nanoscale*, 2011, **3**, 1963–1970.
13 V. Bonacic-Koutecky, A. Kulesza, L. Gell, R. Mitric, R. Antoine, F. Bertorelle, R. Hamouda, D. Rayane, M. Broyer, T. Tabarin and P. Dugourd, *Phys. Chem. Chem. Phys.*, 2012, **14**, 9282–9290.
14 S. Choi, R. M. Dickson and J. Yu, *Chem. Soc. Rev.*, 2012, **41**, 1867–1891.
15 W.-W. Guo, J.-P. Yuan, Q.-Z. Dong and E.-K. Wang, *J. Am. Chem. Soc.*, 2010, **132**, 932–934.
16 E. G. Gwinn, P. O'Neill, A. J. Guerrero, D. Bouwmeester and D. K. Fygenson, *Adv. Mater.*, 2008, **20**, 279–283.
17 J. T. Petty, J. Zheng, N. V. Hud and R. M. Dickson, *J. Am. Chem. Soc.*, 2004, **126**, 5207–5212.
18 J. Zheng and R. M. Dickson, *J. Am. Chem. Soc.*, 2002, **124**, 13982–13983.
19 A. Mathew, P. R. Sajanlal and T. Pradeep, *J. Mater. Chem.*, 2011, **21**, 11205–11212.
20 C. Shao, B. Yuan, H. Wang, Q. Zhou, Y. Li, Y. Guan and Z. Deng, *J. Mater. Chem.*, 2011, **21**, 2863–2866.
21 J. Xie, Y. Zheng and J. Y. Ying, *J. Am. Chem. Soc.*, 2009, **131**, 888–889.
22 H. Wei, Z. Wang, L. Yang, S. Tian, C. Hou and Y. Lu, *Analyst*, 2010, **135**, 1406–1410.
23 H. Hakkinen, *Nat. Chem.*, 2012, **4**, 443–455.
24 J. F. Parker, C. A. Fields-Zinna and R. W. Murray, *Acc. Chem. Res.*, 2010, **43**, 1289–1296.
25 N. Cathcart and V. Kitaev, *J. Phys. Chem. C*, 2010, **114**, 16010–16017.
26 N. Cathcart, P. Mistry, C. Makra, B. Pietrobon, N. Coombs, M. Jelokhani-Niaraki and V. Kitaev, *Langmuir*, 2009, **25**, 5840–5846.
27 S. Kumar, M. D. Bolan and T. P. Bigioni, *J. Am. Chem. Soc.*, 2010, **132**, 13141–13143.
28 J. Guo, S. Kumar, M. Bolan, A. Desireddy, T. P. Bigioni and W. P. Griffith, *Anal. Chem.*, 2012, **84**, 5304–5308.
29 R. Hamouda, B. Bellina, F. Bertorelle, I. Compagnon, R. Antoine, M. Broyer, D. Rayane and P. Dugourd, *J. Phys. Chem. Lett.*, 2010, **1**, 3189–3194.
30 K. M. Harkness, Y. Tang, A. Dass, J. Pan, N. Kothalawala, V. J. Reddy, D. E. Cliffel, B. Demeler, F. Stellacci, O. M. Bakr and J. A. McLean, *Nanoscale*, 2012, **4**, 4269–4274.
31 R. Hamouda, F. Bertorelle, D. Rayane, R. Antoine, M. Broyer and P. Dugourd, *Int. J. Mass Spectrom.*, 2012, **335**, 1–6.
32 G. B. Santiago, M. J. Rodriguez, C. Blanco, J. Rivas, M. A. Lopez-Quintela and J. M. G. Martinho, *Nano Lett.*, 2010, **10**, 4217–4221.
33 B. S. Gonzalez, M. C. Blanco and M. A. Lopez-Quintela, *Nanoscale*, 2012, **4**, 7632–7635.
34 T. Zhou, M. Rong, Z. Cai, C. J. Yang and X. Chen, *Nanoscale*, 2012, **4**, 4103–4106.
35 J. M. Drake, M. L. Lesiecki and D. M. Camaioni, *Chem. Phys. Lett.*, 1985, **113**, 530–534.
36 D. Andrae, U. Haeussermann, M. Dolg, H. Stoll and H. Preuss, *Theor. Chim. Acta*, 1990, **77**, 123–141.
37 S. Gilb, P. Weis, F. Furche, R. Ahlrichs and M. M. Kappes, *J. Chem. Phys.*, 2002, **116**, 4094–4101.
38 A. D. Becke, *Phys. Rev. A*, 1988, **38**, 3098–3100.
39 C. T. Lee, W. T. Yang and R. G. Parr, *Phys. Rev. B: Condens. Matter Mater. Phys.*, 1988, **37**, 789–789.
40 P. J. Stephens, F. J. Devlin, C. F. Chabalowski and M. J. Frisch, *J. Phys. Chem.*, 1994, **98**, 11623–11627.
41 S. J. Vosko, L. Wilk and M. Nusair, *Can. J. Phys.*, 1980, **58**, 1200–1211.
42 T. Yanai, D. P. Tew and N. C. Handy, *Chem. Phys. Lett.*, 2004, **393**, 51–57.
43 M. J. S. Dewar, E. G. Zoebisch, E. F. Healy and J. J. P. Stewart, *J. Am. Chem. Soc.*, 1985, **107**, 3902–3909.
44 X. Le Guével, C. Spies, N. Daum, G. Jung and M. Schneider, *Nano Res.*, 2012, **5**, 379–387.
45 C. Zhou, C. Sun, M. X. Yu, Y. P. Qin, J. G. Wang, M. Kim and J. Zheng, *J. Phys. Chem. C*, 2010, **114**, 7727–7732.
46 L. A. Peyser, A. E. Vinson, A. P. Bartko and R. M. Dickson, *Science*, 2001, **291**, 103–106.
47 L. A. Peyser, T.-H. Lee and R. M. Dickson, *J. Phys. Chem. B*, 2002, **106**, 7725–7728.
48 J. Zheng, P. R. Nicovich and R. M. Dickson, *Annu. Rev. Phys. Chem.*, 2007, **58**, 409–431.
49 S. Huang, C. Pfeiffer, J. Hollmann, S. Friede, J. J. C. Chen, A. Beyer, B. Haas, K. Volz, W. Heimbrodt, J. M. M. Martos, W. Chang and W. J. Parak, *Langmuir*, 2012, **28**, 8915–8919.
50 U. Anand, S. Ghosh and S. Mukherjee, *J. Phys. Chem. Lett.*, 2012, **3**, 3605–3609.
51 I. Chakraborty, T. Udayabhaskararao and T. Pradeep, *Chem. Commun.*, 2012, **48**, 6788–6790.
52 C. Felix, C. Sieber, W. Harbich, J. Buttet, I. Rabin, W. Schulze and G. Ertl, *Chem. Phys. Lett.*, 1999, **313**, 105–109.
53 Z. Sun, Y. Wang, Y. Wei, R. Liu, H. Zhu, Y. Cui, Y. Zhao and X. Gao, *Chem. Commun.*, 2011, **47**, 11960–11962.
54 A. Tlahuice and I. L. Garzon, *Phys. Chem. Chem. Phys.*, 2012, **14**, 7321–7329.
55 B. Bellina, I. Compagnon, F. Bertorelle, M. Broyer, R. Antoine, P. Dugourd, L. Gell, A. Kulesza, R. Mitric and V. Bonacic-Koutecky, *J. Phys. Chem. C*, 2011, **115**, 24549–24554.